0026-895X/10/7705-751–758$20.00
MOLECULAR PHARMACOLOGY
Vol. 77, No. 5
63008/3578030
Mol Pharmacol 77:751–758, 2010
Printed in U.S.A.

Molecular Basis for a High-Potency Open-Channel Block of Kv1.5 Channel by the Endocannabinoid Anandamide

Eloy G. Moreno-Galindo, Gabriel F. Barrio-Echavarría, José C. Vásquez, Niels Decher, Frank B. Sachse, Martin Tristani-Firouzi, José A. Sánchez-Chapula, and Ricardo A. Navarro-Polanco

Centro Universitario de Investigaciones Biomédicas, Universidad de Colima, Colima, México (E.G.M., G.F.B., J.C.V., J.A.S., R.A.N.); Institute of Physiology, Philipps-University, Marburg, Germany (N.D.); and Nora Eccles Harrison Cardiovascular Research and Training Institute (F.B.S., M.T.F.), Department of Bioengineering (F.B.S.), and Division of Pediatric Cardiology (M.T.F.), University of Utah, Salt Lake City, Utah

Received December 7, 2009; accepted January 28, 2010

ABSTRACT

The endocannabinoid, *N*-arachidonoylethanolamine (anandamide; AEA) is known to interact with voltage-gated K^+ (Kv) channels in a cannabinoid receptor-independent manner. AEA modulates the functional properties of Kv channels, converting channels with slowly inactivating current into apparent fast inactivation. In this study, we characterize the mechanism of action and binding site for AEA on Kv1.5 channels expressed on HEK-293 cells using the patch-clamp techniques. AEA exhibited high-potency block ($IC_{50} \approx 200$ nM) from the cytoplasmic membrane surface, consistent with open-channel block. Alanine-scanning mutagenesis revealed that AEA interacts with two crucial β-branching amino acids, Val505 and Ile508 within the S6 domain. Both residues face toward the central cavity and constitute a motif that forms a hydrophobic ring around the ion conduction pathway. This hydrophobic ring motif may be a critical determinant of cannabinoid receptor-independent AEA modulation in other K^+ channel families.

Endocannabinoids are a family of polyunsaturated compounds that are implicated in a wide variety of physiological processes, including memory, blood pressure regulation, immunity, pain, drug addiction, perception, reproduction, and sleep (Martin et al., 1999). *N*-Arachidonoylethanolamine (anandamide; AEA) is an endogenous cannabinoid widely expressed in the nervous system that exerts its effect by activating the G-protein-coupled CB1 and CB2 cannabinoid receptors. Emerging evidence suggests a role for endocannabinoids in the cardiovascular system under pathological conditions, such as hypertension, myocardial infarction, and heart failure (Bátkai and Pacher, 2009).

In addition to directly activating cannabinoid receptors, AEA interacts with several classes of voltage-gated potassium (Kv) channels in a cannabinoid receptor-independent manner (Poling et al., 1996; Van den Bossche and Vanheel, 2000; Oliver et al., 2004; Vignali et al., 2009; Barana et al., 2010). For example, AEA reduces delayed rectifier Kv current and accelerates current decay (Poling et al., 1996; Van den Bossche and Vanheel, 2000; Oliver et al., 2004) in a manner reminiscent of open-channel blockers and Kvβ subunits. AEA inhibits Kv current even while cannabinoid receptors are selectively blocked, indicating a receptor-independent mechanism. The precise mechanism of action and the binding site of AEA on Kv channels remain unclear. Our study focused on the mechanism and structural basis of AEA inhibition of a Kv1 subfamily member, the human delayed rectifier Kv1.5. Our experimental data and molecular modeling support the idea that AEA is a potent, open-channel blocker with binding sites localized to the S6 domain that line the channel vestibule.

This work was supported by the Consejo Nacional de Ciencia y Tecnología, México [Grant CONACyT-054577] and the Nora Eccles Treadwell Foundation.
E.G.M. and G.F.B. contributed equally to this work.
Article, publication date, and citation information can be found at http://molpharm.aspetjournals.org.
doi:10.1124/mol.109.063008.

ABBREVIATIONS: AEA, *N*-arachidonoylethanolamine; Kv, voltage-gated potassium channel; TEA, tetraethylammonium; HEK, human embryonic kidney; WT, wild type; K_4BAPTA, 1,2-bis (2-aminophenoxy)ethane-*N*,*N*,*N*′,*N*′-tetraacetic acid, tetrapotassium salt; S9947, 2′-(benzyloxycarbonylaminomethyl)biphenyl-2-carboxylic acid 2-(2-pyridyl)ethylamide; S0100176, *N*-benzyl-*N*-pyridin-3-ylmethyl-2-(toluene-4-sulfonylamino)-benzamide hydrochloride; AVE0118, 2′-{[2-(4-methoxy-phenyl)-acetylamino]-methyl}-biphenyl-2-carboxylic acid (2-pyridin-3-yl-ethyl)-amide; ICAGEN-4, *N*-[3-(4-ethyl-benzene-sulfonylamino)-2-hydroxy-indan-5-yl]-3-methoxy-benzamide; MSD-D, 2-(4-methoxy-phenyl)-5-methyl-3-oxo-6-*p*-tolylsulfanyl-2,3-dihydro-pyridazine-4-carbonitrile.

Materials and Methods

Human Kv1.5 (*KCNA5*) cDNA was subcloned into pcDNA3.1(+) plasmid (Invitrogen, Carlsbad, CA); this sequence differs from that in the GenBank original database (GenBank accession number NM_002234), which has an N terminus with two additional residues and by the substitution of two residues, K418R and K565E (Decher et al., 2004). Polymerase chain reaction-based site-directed mutagenesis kit (QuikChange; Stratagene, La Jolla, CA) was used to introduce mutations into Kv1.5 cDNA, all of them confirmed by direct DNA sequencing. HEK-293 cells were maintained in Dulbecco's modified Eagle's medium supplemented with 10% horse serum at 37°C in an air/5% CO_2 incubator. Cells were transiently transfected using Lipofectamine 2000 (Invitrogen) according to the supplier's directions. Soluble green fluorescent protein was coexpressed with the channel subunits to identify cells for voltage-clamp experiments.

Electrophysiological Technique and Data Acquisition. Macroscopic currents were recorded in the whole-cell and inside-out configurations of the patch-clamp technique by using an Axopatch-200B amplifier (Molecular Devices, Sunnyvale, CA). All electrophysiological experiments were performed at room temperature (23–24°C). Data acquisition and command potentials were controlled by pClamp 10.0 software (Molecular Devices). Patch pipettes with a resistance of 1.5 to 3 MΩ were made from borosilicate capillary glass (WPI, Sarasota, FL). For whole-cell recordings, patch pipettes were filled with 5 mM K_4BAPTA, 110 mM KCl, 10 mM HEPES, 1 mM $MgCl_2$, and 5 mM ATP-K_2, with pH adjusted to 7.2 with KOH. The standard bath solution contained 130 mM NaCl, 4 mM KCl, 1 mM $MgCl_2$, 10 mM HEPES, 1.8 mM $CaCl_2$, and 10 mM glucose, with pH adjusted to 7.35 with NaOH. Inside-out patches were recorded by using the standard bath solution in the patch pipette, and the perfusing solution contained 135 mM KCl, 1 mM $MgCl_2$, 10 mM HEPES, and 10 mM glucose, with pH adjusted to 7.35 with KOH. The holding potential was −80 mV. The interpulse interval for all the protocols was 30 s to allow channels to fully recover from inactivation between pulses. The voltage-pulse protocols are described under *Results* and in the figure legends.

Drugs. Anandamide (Tocris Bioscience, Ellisville, MO) and TEA (Sigma-Aldrich, St. Louis, MO) were dissolved directly in the probe solution at the desired concentration. HEK-293 cells were exposed to AEA and TEA solutions until steady-state effects were achieved. All other reagents used were from Sigma-Aldrich.

Data Analysis. Data are reported as mean ± S.E.M. (n = number of cells). pClamp 10.0 software (Molecular Devices) was used to perform nonlinear least-squares kinetic analyses of time-dependent currents based on the simplex algorithm. Drug-induced block was measured at the end of 200-ms depolarizing pulses from −80 to + 50 mV. The fractional block of current (f) was plotted as a function of drug concentration ([D]), and the data were fit with a Hill equation: $f = 1/(1 + IC_{50}/[D]^{nH})$ to determine the half-maximal inhibitory concentration (IC_{50}) and the Hill coefficient, n_H. The ratio of current in the presence of drug divided by current before drug ($I_{drug}/I_{control}$) was determined to calculate the fraction of unblocked current as a function of time. When appropriate, Student's paired t test or analysis of variance followed by Bonferroni's test were used for evaluating statistical difference. Significance was assumed for $p < 0.01$ (**) and $p < 0.001$ (***).

Molecular Modeling and Docking. Potential interactions between AEA and the Kv1.5 channel inner vestibule were determined by computational molecular docking. A structural model of the Kv1.5 tetramer developed previously based on the crystal structure of mammalian Shaker Kv1.2 potassium channel subunit complex (Protein Data Bank ID 2a79) was applied (Decher et al., 2008). A structural model of AEA was built, and energy was optimized. The consistent valence force field was used to calculate conformational energies of the AEA and Kv1.5 model. The docking was initiated from random configurations (number of configurations = 200) of AEA in the cytoplasmic cavity of the Kv1.5 tetramer. The docking was performed by using simulated annealing techniques (stages = 50) with an initial temperature of 400 K and a final temperature of 300 K followed by a steepest descent minimization (number of steps = 1000). Kv1.5 segments with residues facing the pore region and AEA were flexible during the optimization procedure. The 10 configurations with minimal energy were studied using interactive three-dimensional visualization. Structural modeling, docking, and visualization were performed with the Insight II modules Homology, Builder, and Docking (version 2005; Accelrys, San Diego, CA).

Results

Concentration- and Voltage-Dependent Inhibition of Kv1.5 Currents by AEA. The effects of AEA on wild-type (WT) Kv1.5 whole-cell currents are illustrated in Fig. 1. With step depolarizations, Kv1.5 current increased rapidly with a sigmoidal time course and then slowly decreased (Fig. 1, A and C). AEA reduced the magnitude of the peak current and the current at the end of the 200-ms pulse in a concentration-dependent manner. In addition, AEA markedly accelerated the rate of current decay (Fig. 1, B and C). For the membrane potentials between −20 and +10 mV, AEA caused a voltage-dependent decrease in macroscopic currents. However, for membrane potentials >+10 mV, in which channels are fully activated, the effect of AEA was no longer voltage-dependent, suggesting that AEA modified steps in the activation pathway (Fig. 1E). Next, we examined the effect of AEA on the rate of current deactivation. Under control conditions, Kv1.5 currents deactivated with a biexponential time course, the fast (τ_f) and the slow (τ_s) time constants averaging 8.1 ± 1.8 and 35 ± 4.6 ms, respectively (n = 9 cells). In the presence of AEA 3 and 10 μM, time constants were τ_f = 7.8 ± 2.1 ms and τ_s = 67 ± 9.2 ms, and τ_f = 9.8 ± 2.4 ms and τ_s = 104 ± 11.6 ms, respectively. The slow deactivation induced by AEA resulted in a crossover phenomenon (Fig. 1F), typical of the "foot-in-the-door" open-channel blocking effect (Yeh and Armstrong, 1978; Snyders et al., 1992). These observations suggest that AEA inhibited Kv1.5 current by an open-channel block mechanism (Armstrong, 1969; Snyders et al., 1992).

Internal TEA Competes with AEA. Classical open-channel blockers access the internal channel pore from the intracellular membrane face. Hence, externally applied open-channel blockers must permeate the membrane before exerting their effect. As an initial approach to determine the sidedness of current inhibition by AEA, we used a cell-attached configuration. In this condition, a compound that acts at an external site on the channel would have no effect on measured current because channels within the patch would not be exposed to bath-applied compound. By contrast, a membrane-permeable open-channel blocker would easily reach the internal site to affect current in the cell-attached configuration. The bath application of AEA reduced Kv1.5 current in the cell-attached mode in a manner similar to the whole-cell configuration (Fig. 2, A and B), supporting the idea that AEA blocks channels from the inside.

In addition, if AEA blocks within the permeation pathway, then a second blocker with overlapping binding sites should compete with AEA for access to the pore. TEA is a membrane-impermeant cation that blocks Kv channels with two distinct binding sites localized at the intra- and extracellular side of the selectivity filter (MacKinnon and Yellen, 1990; Choi et al., 1993). Kv1.5 current recorded at +50 mV was inhibited by ~50% with the external application of 50 mM

TEA or 1 mM internal application (data not shown). External TEA application did not influence Kv1.5 inhibition by AEA (Fig. 2, C and E–G). By contrast, internal TEA modified the potency and the kinetics of inhibition by AEA (Fig. 2, D and E–G). AEA (10 μM) reduced ~80% of the control current, but only 35% of current in the presence of internal TEA (Fig. 2, D and F). The ratio $I_{AEA}/I_{control\ or\ TEA}$ as a function of time during the pulse was used to estimate the rate of onset of block (Fig. 2E). Internal TEA slowed the onset of AEA block, compared with whole-cell, cell-attached, and external TEA conditions (Fig. 2, E and G). These results imply that AEA and TEA compete for overlapping binding sites accessible only from the intracellular site of the membrane.

Anandamide Acts from the Cytoplasmic Membrane Side. To further determine whether AEA acts from the extracellular or intracellular membrane surface, macroscopic inside-out current recordings were performed. Similar to whole-cell experiments, the effect of AEA on macroscopic inside-out currents was time- and concentration-dependent (Fig. 3A). However, we found a dramatic increase of AEA potency with internal application (Fig. 3, A and B). Cytoplasmic application of AEA was 10-fold more potent (IC_{50} = 213 ± 34 nM) than external application (IC_{50} = 2.1 ± 0.44 μM, $p < 0.01$). Under both experimental conditions, the n_H values were close to unity, averaging 1.09 ± 0.06 and 0.83 ± 0.05 for whole-cell and inside-out, respectively (Fig. 3B). The time to reach the steady-state current block (diary plot) was significantly faster when AEA was applied to the intracellular side ($t_{1/2}$ = 1.8 ± 0.16 min) compared with external application of AEA ($t_{1/2}$ = 3.7 ± 0.21 min, $p < 0.01$). Moreover, the current was almost totally recovered after washout in the inside-out but not in the whole-cell configuration (Fig. 3C). Next, we added AEA 10 μM in the inside-out pipette solution to restrict its action on the external membrane face while maintaining a continuous bath superfusion to wash off AEA that diffused across the membrane. Under these conditions, AEA did not inhibit the Kv1.5 current until it was directly applied to the internal bath solution (Fig. 3D). All of these observations strongly support the idea that AEA inhibits its Kv1.5 current from the cytoplasmic membrane face.

Concentration-Dependent Kinetics of Kv1.5 Current Block. The ratio $I_{AEA}/I_{control}$ as a function of time during sustained depolarizations at +50 mV was used to estimate initial block and quantify the kinetics of AEA block (Fig. 4). The respective current ratio starts at values close to 1, indicating that channel block occurs just after channel opening. This result also indicates that channels recovered completely from block during the 30-s interval between depolarizations. Block increased exponentially during depolarization, and the time constant of this process was faster at higher AEA concentrations (Fig. 4A). The linear relationship between the rate of channel block ($1/\tau_{block}$) and AEA concentration (Fig. 4B) indicates that the rate of block is a good approximation to drug-channel interaction kinetics. The best least-squares fit to the data resulted in an apparent association (k_{on}) and dissociation (k_{off}) rate constants values of 0.093 ± 0.01 $nM^{-1} \cdot s^{-1}$ and 18.9 ± 5.2 s^{-1}, respectively. The quotient of these rate constants (k_{off}/k_{on}) gives a K_D value of 203 nM, very similar to the IC_{50} (213 nM) calculated from concentration-response curves obtained in the inside-out configuration.

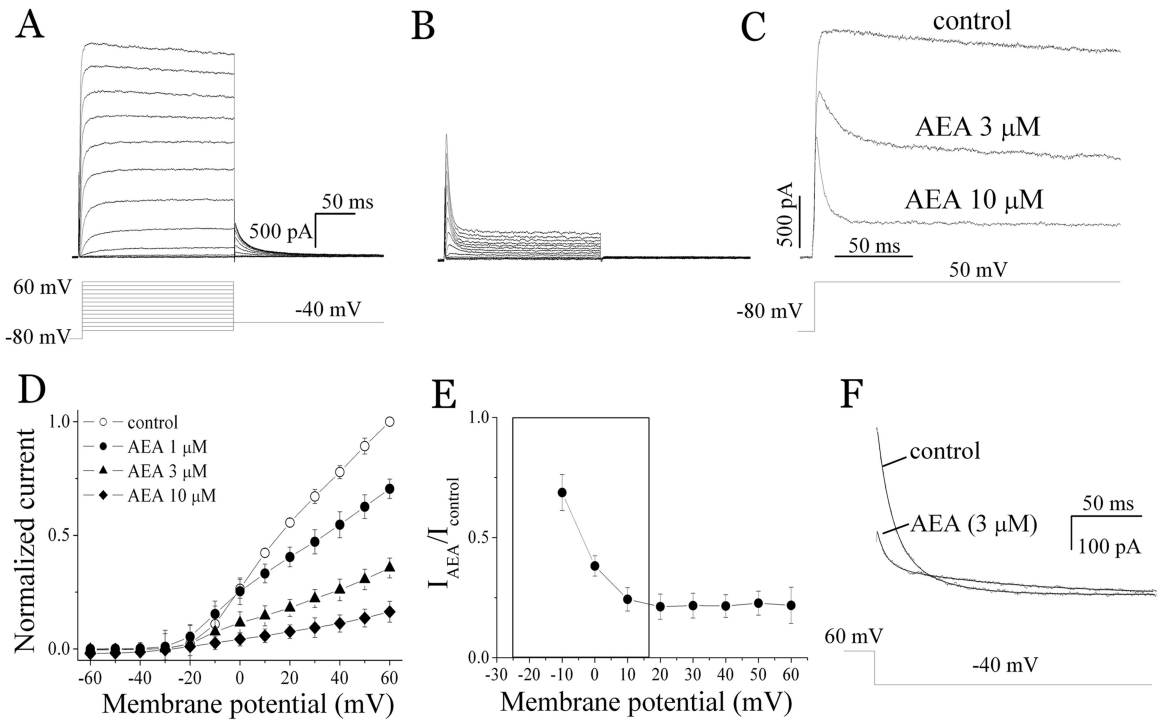

Fig. 1. Effects of AEA on WT Kv1.5 channel. Whole-cell currents recorded from transfected HEK-293 cells before (A) and after (B) extracellular application of AEA (10 μM). Currents were elicited by 200-ms depolarizations from a holding potential of −80 mV to test potentials between −60 to +60 mV in 10-mV steps. Test potential was followed by a repolarizing step to −40 mV to record deactivation currents. C, superimposed current traces obtained after depolarization to +50 mV in the absence and presence of the indicated concentrations of AEA. D, current-voltage relationships for currents measured at the end of the 200-ms test pulse before and after application of AEA (n = 6). E, fractional block of channel currents, measured at the end of 200-ms pulses and plotted as a function of test potential. F, superimposed tail currents obtained upon repolarization to −40 mV in the absence and in the presence of AEA.

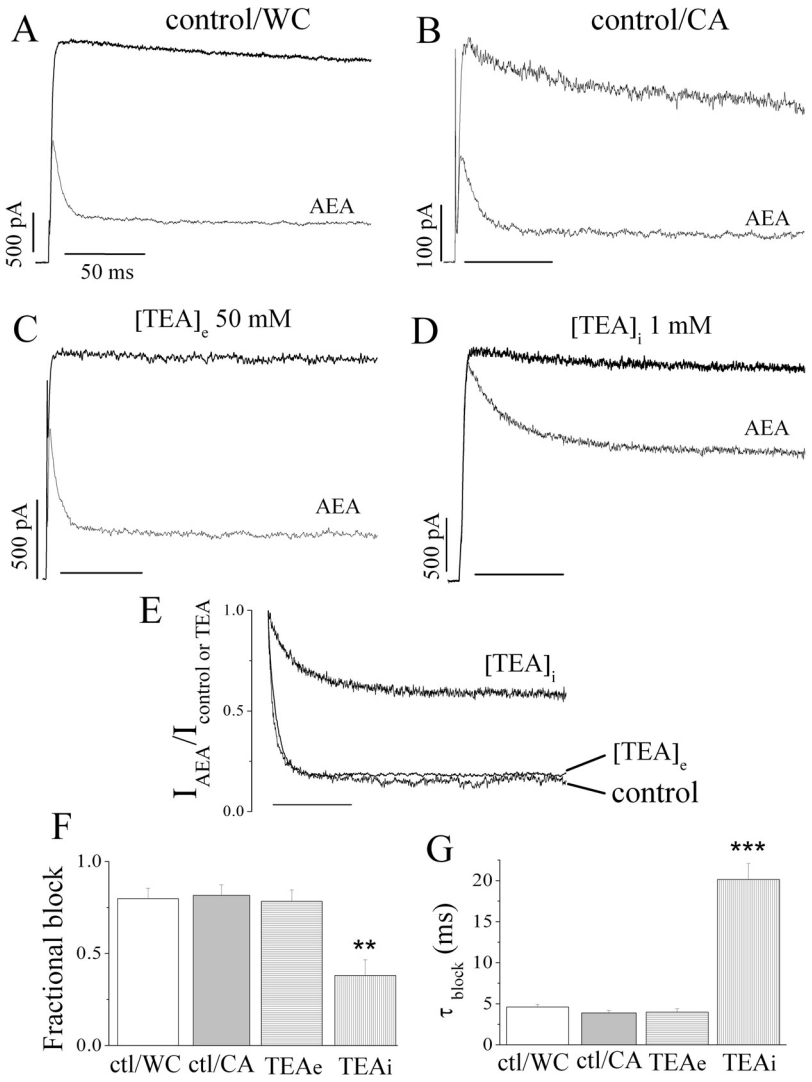

Fig. 2. AEA and internal TEA competition. Superimposed WT Kv1.5 current traces obtained by 200-ms depolarization to +50 mV from a holding potential of −80 mV (A–D). AEA (10 μM) was applied in whole-cell (A, C, and D) and cell-attached (B) configurations, in the absence (A and B) and in the presence of the indicated concentrations of TEA, applied externally (C) or in the pipette solution (D). The TEA concentrations (internal and external) carry out ~50% of current block. E, plot of the onset of channel block ($I_{AEA}/I_{control\ or\ TEA}$) during 200-ms pulses shown in A, C, and D. Note that at time 0 there is no block of current ($I_{drug}/I_{control} = 1$). The time constant describing the rate of onset channel block was determined by a single exponential fit of the current ratio. F, the fraction of the channel blocked was calculated measuring at the end of the onset of channel block. G, comparative values of time constants of block (τ_{block}) obtained from monoexponential fits under the three experimental conditions. Columns and error bars (F and G) correspond to means ± S.E.M. (n = 5–7) obtained in the four experimental conditions described.

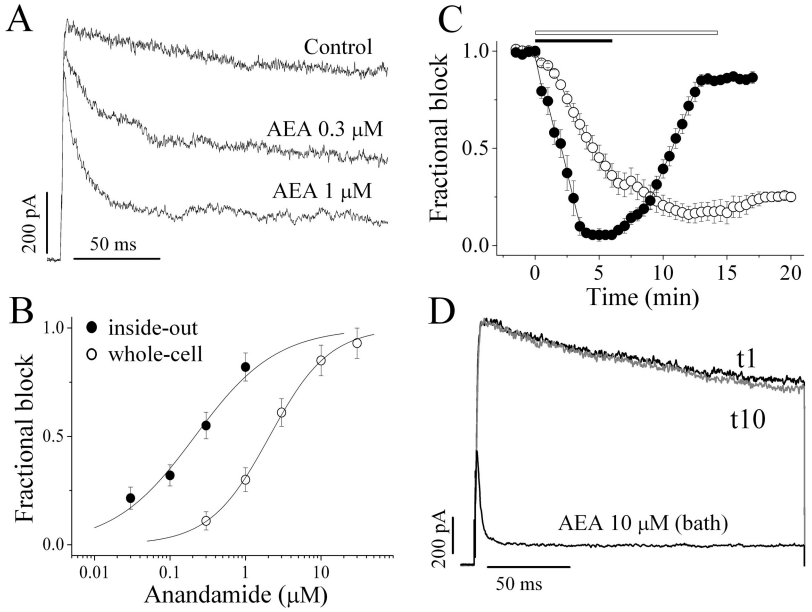

Fig. 3. AEA blocks the current channel from the intracellular leaflet of membrane. A, superimposed inside-out recordings obtained by 200-ms depolarizations to +50 mV from a holding potential of −80 mV, in the absence and presence of the indicated concentrations of AEA. B, concentration-dependence of AEA-induced block of WT Kv1.5 channels in whole-cell (○) and inside-out (●) configurations. The continuous lines represent the fit to the experimental data using the Hill equation. C, time course plot showing block of channel by 10 μM AEA in whole-cell (○) and inside-out (●) configurations. Channel currents were measured at the end of 200-ms pulses to +50 mV applied every 30 s. Each circle correspond to mean ± S.E.M. (n = 7–9) obtained before, during, and after application of AEA to bath solution. The duration of the AEA application is indicated by closed and open bars for inside-out and whole-cell configurations, respectively. Note that the current was almost totally recovered using only the inside-out configuration. D, inside-out macroscopic currents obtained with 10 μM AEA in the pipette solution and using a described previously protocol described previously (Fig. 1C). Current traces were recorded immediately after obtaining the inside-out configuration (t1), 10 min later (t10), and subsequent to perfusing AEA in bath solution. Similar results were obtained in all of the nine cells tested.

Two Amino Acids in the Kv1.5 S6 Domain Comprise the AEA Binding Site. Residues in the S6 transmembrane domain that face the inner cavity of Kv channels have been identified as a common binding site for several drugs that act like open-channel blockers (Yeola et al., 1996; Mitcheson et al., 2000; Decher et al., 2004). Therefore, 21 residues located in the S6 domain (Gly497 to Ser517) or between the pore helix and the selectivity filter were mutated to alanine (native alanine residues were not modified). In this experimental series, whole-cell configuration was used because several mutant channels showed low expression. To determine the degree of block for each mutant channel, currents at the end of 200-ms pulses at +50 mV were measured before and after the application of AEA (10 μM). At this concentration, WT Kv1.5 current was blocked 81% (Fig. 5). Mutants V505A and I508A significantly reduced ($p < 0.001$) the potency of AEA block (Fig. 5, A and B); the IC_{50} was increased 15.8-fold for V505A and 14.5-fold for I508A (Fig. 5C). It is interesting that the I502A mutant showed a small and brief decaying transient after channel opening even though the potency of AEA block was similar to the observed in WT channel (Fig. 5B). On the other hand, one of the most important drug-binding site for several Kv1.5 open-channel blockers (Val512) (Decher et al., 2004, 2006; Strutz-Seebohm et al., 2007; Aréchiga et al., 2008) did not seem to be important in the interaction with AEA. To further analyze the effect of AEA on I502A, V505A, and I508A mutant channels, the time course of block ($I_{drug}/I_{control}$) for each mutant was plotted (Fig. 6). Similar to WT, the current ratio for these mutants start at values close to 1, indicating that channel block proceeds after channel opening (Fig. 6, B–D). For the mutants less sensitive to AEA (V505A and I508A), the time course of the current ratio was biphasic, with an initial rapid phase of block followed by a slower partial recovery from block. The time constants for the rate of onset of block were significantly reduced for I502A, V505A, and I508A compared with WT (Fig. 6A). The time constants of recovery from block were 8.72 ± 1.23 and 267 ± 15.3 ms for mutants V505A and I508A, respectively.

Molecular Modeling of AEA within the Kv 1.5 Pore Domain. Molecular modeling was used to identify the energy-minimized conformation of AEA within the conduction pathway of the Kv1.5 open channel. AEA is an inherently flexible

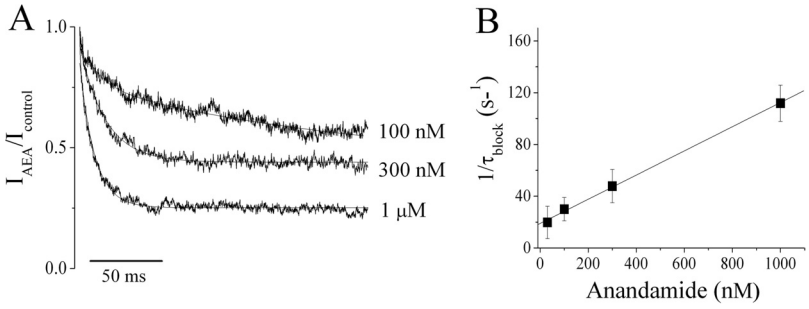

Fig. 4. Concentration-dependent kinetics of AEA block. A, inside-out superimposed traces of the ratio $I_{AEA}/I_{control}$ during 200 ms are shown for 0.1, 0.3, and 1 μM AEA. Solid lines indicate the best fit to a single exponential function. B, relationship between $1/\tau_{block}$ and AEA concentration. τ_{block} values were obtained from the fit of the sensitive current ($I_{AEA}/I_{control}$) at different AEA concentrations. Each point represents the mean ± S.E.M. ($n = 8$). For a first-order blocking scheme, a linear relationship is expected: $1/\tau_{block} = k_{on} \times [AEA] + k_{off}$. Solid line represents fit to the data with a linear function, from which the apparent binding (k_{on}) and unbinding (k_{off}) rate constants were obtained.

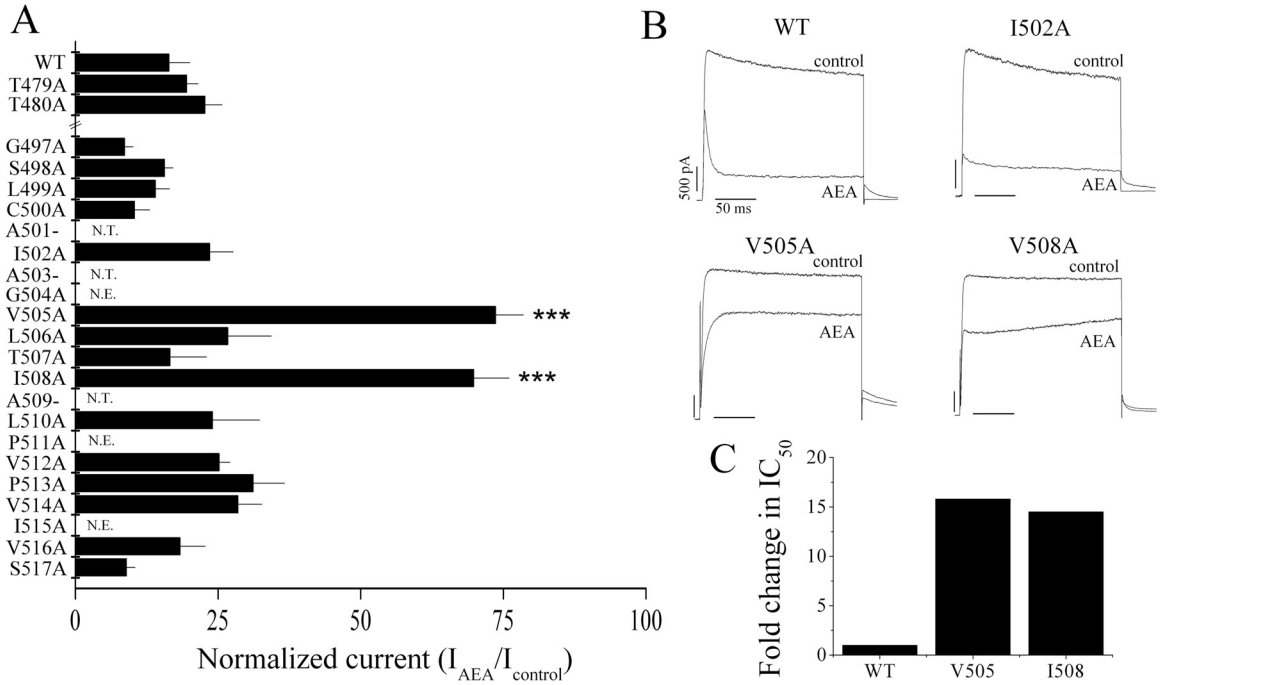

Fig. 5. Localization of the putative AEA binding site. A, WT and mutant Kv1.5 channels were activated by 200-ms pulses to +50 mV every 30 s. AEA (10 μM) was perfused, and the steady-state inhibition of Kv1.5 was calculated as the percentage of reduction of the current at the end of a 200-ms pulse ($n = 4–8$). B, representative current traces recorded in the absence (control) and presence of AEA for WT and the indicated mutant channels. Note that block induced by AEA on I502A and WT was similar; however, in this mutant, the time-dependent component was virtually absent. C, changes in IC_{50} caused by mutations at the putative Kv1.5 binding sites of AEA. NT, not tested residues; NE, nonexpressing mutant channel; ***, $p < 0.001$, compared with WT Kv1.5.

molecule that can assume a variety of conformations (Barnett-Norris et al., 1998; Lynch and Reggio, 2005). In the minimal energy pose, AEA adopts a complex conformation consisting of a linear component associated with the alkyl tail and a series of hairpin loops within the double-bond acyl region, extending toward the head group (Fig. 7). The hairpin loops and head group adopt a compact structure resembling a "hydrophobic ball." The hydrophobic ball is nestled within a hydrophobic ring comprised by residues Val505 and Ile508 from each of the four subunits. Molecular modeling predicted multiple hydrophobic interactions between the hydrogen atoms of Val505 and Ile508 side chains and hydrogen atoms within the double-bond acyl region of AEA. The distances between the hydrogen atoms on Val505/Ile508 and AEA varied between 2.6 and 2.9 Å. The hydrophobic ball portion of AEA occupied a position within the center of the ion conduction pathway, which would be predicted to inhibit K^+ flux by plugging the pore. By contrast, the alkyl tail was aligned along the S6 domain, extending toward the PVP motif. Examination of the 10 lowest-energy docking results consistently demonstrated the compact, hairpin-looped AEA conformation nestled within the hydrophobic ring composed of Val505/Ile508 and a linear alkyl tail extending toward the PVP motif.

Discussion

Emerging evidence suggests a role for endocannabinoids in pathogenesis of a variety of cardiovascular disorders, including systemic and pulmonary hypertension, myocardial infarction, and heart failure (Bátkai and Pacher, 2009). The observation that endocannabinoids act in a cannabinoid receptor-independent manner opens the possibility that endocannabinoids may directly influence Kv channel function in pathological cardiovascular conditions. In this context, we sought to determine the precise mechanism of action and binding site of the endogenous cannabinoid AEA on human Kv1.5 channels. While our article was in preparation, Barana et al. (2010) reported that endocannabinoids, including AEA, inhibit Kv1.5 channels stably expressed in a mouse fibroblast cell line. These authors report that the AEA binding site is localized to the external vestibule of the Kv1.5 channel. By contrast, our data support the idea the AEA functions as an open-channel blocker with binding sites localized to the internal line of the channel pore.

In our study and that of Barana et al. (2010), several lines of evidence suggest that AEA behaves as an open-channel blocker of Kv1.5 channels. First, block occurred after channel opening, increased steeply in the voltage range of channel activation, and was voltage-independent at voltages in which the channel is fully activated. Moreover, AEA slowed Kv1.5 current deactivation, resulting in tail current crossover. This observation suggests that AEA binding interferes with the closure of activation gate, a phenomenon called the "foot-in-the-door" effect (Yeh and Armstrong, 1978). In addition, the effect of externally applied AEA was not reversible with prolonged washing. By contrast, we found that the effect of internal AEA application was reversible. Moreover, AEA was 10-fold more potent when applied to the cytoplasmic face compared with external application.

The ability of two compounds to compete for access to their respective binding sites allows for the determination of an intracellular or extracellular mechanism of action. In this light, TEA is an excellent probe given that the location of the intra- and extracellular binding sites are well described. Barana et al. (2010) reported that internal TEA did not affect AEA inhibition, whereas external TEA reduced the degree of AEA current inhibition. However in our study, external TEA did not influence the ability of AEA to reduce Kv1.5 current. In contrast, internal TEA application slowed the rate of current decline and reduced the magnitude of AEA-induced current inhibition. In addition, the inability of AEA to inhibit the current when it was restricted to the external membrane face (Fig. 3D) suggests that AEA does not exert an external effect on the WT channel. Hence, a possible explanation for the less sensitive mutant R487Y reported by Barana et al. (2010) is

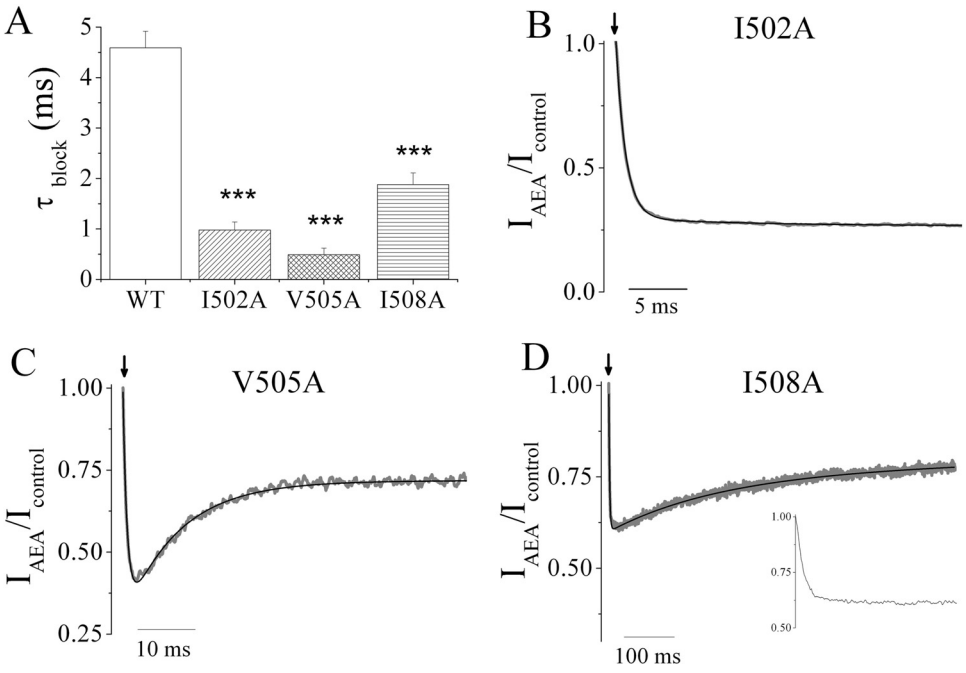

Fig. 6. Block of Kv1.5 mutants that affect the potency and kinetics of AEA block. A, time constants for onset of block (τ_{block}) obtained from the mutants I502A, V505A, and I508A (WT value from Fig. 2G is shown for comparison purposes). Representative onset of current block by 10 μM AEA assessed during depolarizing pulses to +50 mV for the mutants I502A (B), V505A (C), and I508A (D). The continuous line represents a single (B) or biexponential (C and D) fit of the experimental data. Insert shows the first 30 ms of the current block onset. Arrow represents time 0.

an allosteric effect induced by this mutation transmitted to the S6 segment.

A number of residues in the Kv1.5 pore helix and S6 domain have been identified as important components of the drug-binding site for several blockers (Decher et al., 2004, 2006; Eldstrom et al., 2007; Strutz-Seebohm et al., 2007; Aréchiga et al., 2008). In contrast to other blockers, residues in the deep pore/pore helix (Thr479/Val480) were not important as binding sites for AEA based on site-directed mutagenesis and molecular modeling. However, we identified two mutations (V505A and I508A) in the lower portion of the S6 domain that markedly reduced AEA block. Val505 and Ile508 are also key residues in interaction with Kv1.5 channel blockers AVE0118, S0100176, vernakalan (Decher et al., 2004, 2006; Eldstrom et al., 2007) and the Kvβ1.3 N terminus (Uebele et al., 1998; Gulbis et al., 1999). Furthermore, Ile508 constitutes an important residue of the binding site for drugs ICAGEN-4, MSD-D, and S9947 (Strutz-Seebohm et al., 2007). Thus, the key binding sites for AEA overlap with a subset of residues important for binding of other Kv1.5 channel blockers.

It has been proposed that β-branched amino acids valine, isoleucine, or threonine located (i, i + 3) or (i, i + 4) apart on an α helix can form an important interaction motif for cannabinoid ligands (Barnett-Norris et al., 2002). Indeed, molecular modeling and structure-function studies reveal that the interaction between AEA and the CB1 receptor involves a hydrophobic motif, Val6.43/ Ile6.46 (Patricelli and Cravatt, 2001; Lynch and Reggio, 2005, 2006). Our mutational analysis revealed that the two residues critical for the AEA inhibition, Val505 and Ile508, also form a hydrophobic motif. As a result of the symmetry of the tetrameric channel, this motif forms a hydrophobic ring that encircles the ion conduction pathway. Molecular modeling suggests that AEA adopts a compact, hair-pinned conformation that extends from the double-carbon bonds toward the head group, essentially forming a hydrophobic ball. In the minimal energy pose, the hydrophobic ball region of AEA is centered within the ion conduction pathway, stabilized by hydrophobic interactions with Val505 and Ile508 side chain hydrogen atoms from each of the four subunits. Thus, stabilization of the hydrophobic ball of AEA within the hydrophobic ring of the channel essentially plugs the ion conduction pathway. The alkyl tail of AEA aligns itself along the S6 domain of a single subunit in an extended conformation close to the PVP motif. This proximity might interfere with channel closure, resulting in the observed crossover of deactivating tail current in the presence of AEA. A similar foot-in-the-door mechanism was proposed for Kv1.5 block by AVE0118, which also adopts a configuration that extends toward the PVP motif (Decher et al., 2006).

Multiple AEA conformations, including the complex conformation described here, have been reported in previous molecular dynamic simulations (Barnett-Norris et al., 1998; Lynch and Reggio, 2005). We propose that AEA blocks Kv1.5 channels by occupying a position within the ion conduction pathway and essentially plugging the pore. The Val505/ Ile508 motif is highly conserved in Kv family members and may explain their susceptibility to AEA and other highly unsaturated lipids (Poling et al., 1996; Oliver et al., 2004, McKay and Worley, 2001). By contrast, channels known to be insensitive to highly unsaturated lipids, such as Kv7.2/7.3 (KCNQ) and large-conductance voltage/Ca^{2+}-gated channels, lack this motif (Fig. 8) (Oliver et al., 2004).

In addition to reducing the potency of AEA inhibition, V505A and I508A mutants also altered the kinetic properties

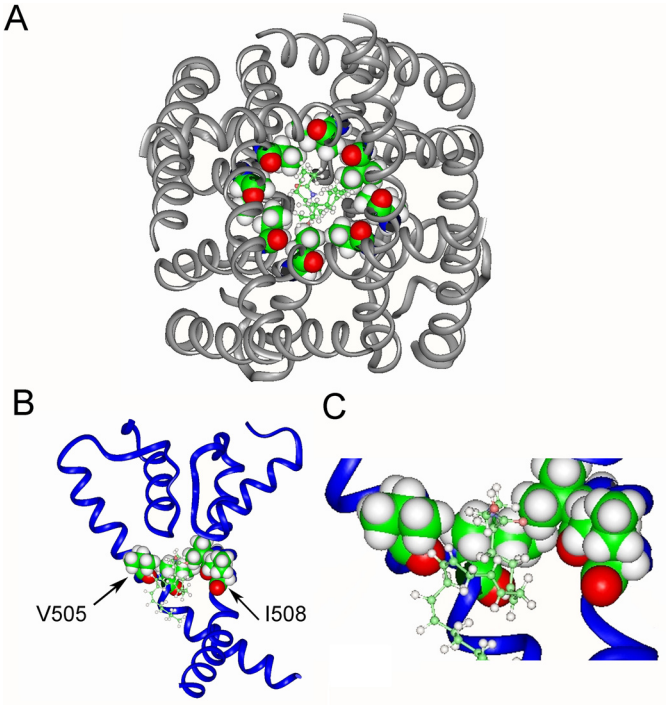

Fig. 7. Docking of AEA within the Kv1.5 channel inner vestibule. A, cytoplasmic view of the Kv1.5 channel inner pore focusing on the Ser6 helices to highlight the hydrophobic ring composed by Val505 and Ile508 from each subunit. AEA is docked within the ion conduction pathway, stabilized within the hydrophobic ring. The Ser6 helices are depicted as silver ribbons. The side chains of Val505 and Ile508 are depicted as space-filled balls (individual atoms are colored as follows: carbon, green; hydrogen, white; oxygen, red). B, side view of two adjacent Kv1.5 subunits, showing the pore helix, selectivity filter, and S6 domains. The side chains of Val505 and Ile508 are depicted as space-filled balls. C, enlarged view of B highlighting the hairpin loops within the double-bond acyl region of AEA. The hairpin loops are nestled within the hydrophobic ring, whereas the alkyl tail is aligned along the S6 domain of a single subunit.

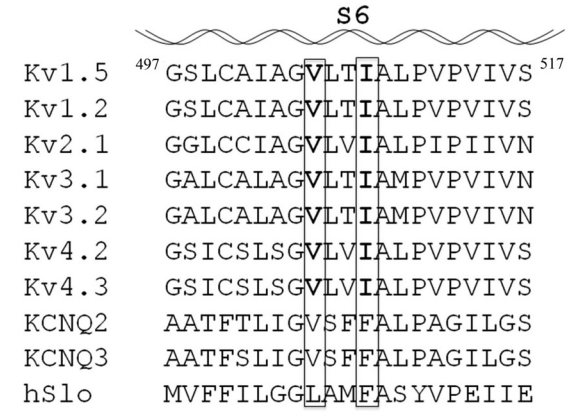

Fig. 8. Amino acid sequence alignment of part of the S6 domain for several potassium channels. The hydrophobic motif (boxed boldface letters) is noted. All shown sequences correspond to *Homo sapiens*: Kv1.5 (GI: 25952087), Kv1.2 (GI: 4826782), Kv2.1 (GI: 4826784), Kv3.1 (GI:163792201), Kv 3.2 (GI:21217561), Kv4.2 (GI:6006517), Kv4.3 (GI: 6007797), KCNQ2/ Kv7.2, (GI:66347344), KCNQ3/Kv7.3 (GI:5921785), hSLo/large-conductance voltage/Ca^{2+}-gated channels, (GI:46396283).

of drug block. Both mutations accelerated the initial onset of drug block (Fig. 6), giving the appearance of the absence of a time-dependent component of block in the macroscopic currents (Fig. 5B). It is interesting that a similar phenomenon was reported for open-channel block of Kv1.5 channels by quinine (Snyders and Yeola, 1995). However for both mutations, the rapid block was followed by partial recovery from block. We speculate that mutation of either key binding site residue reduces the overall number of hydrophobic contacts with AEA, thus destabilizing the AEA hydrophobic ball within the ion-conduction pathway. Both mutations may reduce the initial steric hindrance of AEA binding and thereby accelerate the onset of initial block. Likewise, I502A increased the rate of AEA block but did not affect the potency. Mutation of this residue was proposed to alter the side chain orientation of nearby residues and disrupt drug-channel interactions through an allosteric mechanism (Decher et al., 2004).

In summary, we found that the endocannabinoid AEA is a high-potency intracellular blocker of Kv1.5 channels. The current decay induced by AEA is not a result of modulation of intrinsic inactivation gating (Oliver et al., 2004) but rather open-channel block. AEA blocks ion permeation by plugging the intracellular channel vestibule, stabilized by a ring of hydrophobic residues in the S6 domain. These findings support the hypothesis that AEA acts as an intracellular messenger capable of modulating channel activity (van der Stelt and Di Marzo, 2005). The conserved valine-isoleucine hydrophobic motif typical for several classes of Kv channels suggests a possible structural explanation for a more general mechanism of interaction between K^+ channels and endocannabinoids.

Acknowledgments

We thank Miguel Angel Flores for technical assistance.

References

Aréchiga IA, Barrio-Echavarria GF, Rodríguez-Menchaca AA, Moreno-Galindo EG, Decher N, Tristani-Firouzi M, Sánchez-Chapula JA, and Navarro-Polanco RA (2008) Kv1.5 open channel block by the antiarrhythmic drug disopyramide: molecular determinants of block. *J Pharmacol Sci* **108:**49–55.

Armstrong CM (1969) Inactivation of the potassium conductance and related phenomena caused by quaternary ammonium ion injection in squid axons. *J Gen Physiol* **54:**553–575.

Barana A, Amorós I, Caballero R, Gómez R, Osuna L, Lillo MP, Blázquez C, Guzmán M, Delpón E, and Tamargo J (2010) Endocannabinoids and cannabinoid analogues block cardiac hKv1.5 channels in a cannabinoid receptor-independent manner. *Cardiovasc Res* **85:**56–67.

Barnett-Norris J, Guarnieri F, Hurst DP, and Reggio PH (1998) Exploration of biologically relevant conformations of anandamide, 2-arachidonylglycerol, and their analogues using conformational memories. *J Med Chem* **41:**4861–4872.

Barnett-Norris J, Hurst DP, Buehner K, Ballesteros JA, Guarnieri F, and Reggio PH (2002) Agonist alkyl tail interaction with cannabinoid CB1 receptor V6.43/I6.46 groove induces a helix 6 active conformation. *Int J Quantum Chem* **88:**76–86.

Bátkai S and Pacher P (2009) Endocannabinoids and cardiac contractile function: pathophysiological implications. *Pharmacol Res* **60:**99–106.

Choi KL, Mossman C, Aubé J, and Yellen G (1993) The internal quaternary ammonium receptor site of *Shaker* potassium channels. *Neuron* **10:**533–541.

Decher N, Gonzalez T, Streit AK, Sachse FB, Renigunta V, Soom M, Heinemann SH, Daut J, and Sanguinetti MC (2008) Structural determinants of Kvbeta1.3-induced channel inactivation: a hairpin modulated by PIP2. *EMBO J* **27:**3164–3174.

Decher N, Kumar P, Gonzalez T, Pirard B, and Sanguinetti MC (2006) Binding site of a novel Kv1.5 blocker: a "foot in the door" against atrial fibrillation. *Mol Pharmacol* **70:**1204–1211.

Decher N, Pirard B, Bundis F, Peukert S, Baringhaus KH, Busch AE, Steinmeyer K, and Sanguinetti MC (2004) Molecular basis for Kv1.5 channel block: conservation of drug binding sites among voltage-gated K^+ channels. *J Biol Chem* **279:**394–400.

Eldstrom J, Wang Z, Xu H, Pourrier M, Ezrin A, Gibson K, and Fedida D (2007) The molecular basis of high-affinity binding of the antiarrhythmic compound vernakalant (RSD1235) to Kv1.5 channels. *Mol Pharmacol* **72:**1522–1534.

Gulbis JM, Mann S, and MacKinnon R (1999) Structure of a voltage-dependent K^+ channel beta subunit. *Cell* **97:**943–952.

Lynch DL and Reggio PH (2005) Molecular dynamics simulations of the endocannabinoid *N*-arachidonoylethanolamine (anandamide) in a phospholipid bilayer: probing structure and dynamics. *J Med Chem* **48:**4824–4833.

Lynch DL and Reggio PH (2006) Cannabinoid CB1 receptor recognition of endocannabinoids via the lipid bilayer: molecular dynamics simulations of CB1 transmembrane helix 6 and anandamide in a phospholipid bilayer. *J Comput Aided Mol Des* **20:**495–509.

MacKinnon R and Yellen G (1990) Mutations affecting TEA blockade and ion permeation in voltage-activated K+ channels. *Science* **250:**276–279.

McKay MC and Worley JF 3rd (2001) Linoleic acid both enhances activation and blocks Kv1.5 and Kv2.1 channels by two separate mechanisms. *Am J Physiol Cell Physiol* **281:**C1277–C1284.

Martin BR, Mechoulam R, and Razdan RK (1999) Discovery and characterization of endogenous cannabinoids. *Life Sci* **65:**573–595.

Mitcheson JS, Chen J, Lin M, Culberson C, and Sanguinetti MC (2000) A structural basis for drug-induced long QT syndrome. *Proc Natl Acad Sci USA* **97:**12329–12333.

Oliver D, Lien CC, Soom M, Baukrowitz T, Jonas P, and Fakler B (2004) Functional conversion between A-type and delayed rectifier K^+ channels by membrane lipids. *Science* **304:**265–270.

Patricelli MP and Cravatt BF (2001) Characterization and manipulation of the acyl chain selectivity of fatty acid amide hydrolase. *Biochemistry* **40:**6107–6115.

Poling JS, Rogawski MA, Salem N Jr., and Vicini S (1996) Anandamide, an endogenous cannabinoid, inhibits Shaker-related voltage-gated K^+ channels. *Neuropharmacology* **35:**983–991.

Snyders DJ and Yeola SW (1995) Determinants of antiarrhythmic drug action. Electrostatic and hydrophobic components of block of the human cardiac hKv1.5 channel. *Circ Res* **77:**575–583.

Snyders J, Knoth KM, Roberds SL, and Tamkun MM (1992) Time-, voltage-, and state-dependent block by quinidine of a cloned human cardiac potassium channel. *Mol Pharmacol* **41:**322–330.

Strutz-Seebohm N, Gutcher I, Decher N, Steinmeyer K, Lang F, and Seebohm G (2007) Comparison of potent Kv1.5 potassium channel inhibitors reveals the molecular basis for blocking kinetics and binding mode. *Cell Physiol Biochem* **20:**791–800.

Uebele VN, England SK, Gallagher DJ, Snyders DJ, Bennett PB, and Tamkun MM (1998) Distinct domains of the voltage-gated K^+ channel Kv beta 1.3 beta-subunit affect voltage-dependent gating. *Am J Physiol* **274:**C1485–C1495.

Van den Bossche I and Vanheel B (2000) Influence of cannabinoids on the delayed rectifier in freshly dissociated smooth muscle cells of the rat aorta. *Br J Pharmacol* **131:**85–93.

van der Stelt M and Di Marzo V (2005) Anandamide as an intracellular messenger regulating ion channel activity. *Prostaglandins Other Lipid Mediat* **77:**111–122.

Vignali M, Benfenati V, Caprini M, Anderova M, Nobile M, and Ferroni S (2009) The endocannabinoid anandamide inhibits potassium conductance in rat cortical astrocytes. *Glia* **57:**791–806.

Yeh JZ and Armstrong CM (1978) Immobilisation of gating charge by a substance that simulates inactivation. *Nature* **273:**387–389.

Yeola SW, Rich TC, Uebele VN, Tamkun MM, and Snyders DJ (1996) Molecular analysis of a binding site for quinidine in a human cardiac delayed rectifier K+ channel. Role of S6 in antiarrhythmic drug binding. *Circ Res* **78:**1105–1114.

Address correspondence to: Dr. Ricardo A. Navarro-Polanco, Centro Universitario de Investigaciones Biomédicas, Universidad de Colima, Av. 25 de Julio 965, col. Villa San Sebastian, Colima, Col., Mexico. C.P. 28045. E-mail: magdal@ucol.mx